ISSN 1995-0780, Nanotechnologies in Russia, 2018, Vol. 13, Nos. 3–4, pp. 109–115. © Pleiades Publishing, Ltd., 2018.

NANOSTRUCTURES, INCLUDING NANOTUBES

Microwave Assisted Synthesis and Oxidation Resistance of Sm^{3+} Doped Fe_3O_4 Nanoparticles[1]

O. E. Polozhentsev[a]*, V. V. Butova[a], V. K. Kochkina[a], and A. V. Soldatov[a]

[a] *Smart Materials Research Center, Southern Federal University, Rostov-on-Don, 344090 Russia*

**e-mail: olegpolozhentsev@mail.ru*

Received November 1, 2017; in final form, April 13, 2018

Abstract—In this study, pure and Sm^{3+} doped Fe_3O_4 nanoparticles were prepared via a microwave assisted synthesis in water solution. The samples were characterized by TEM, XRD, XANES, and VSM techniques. The structure and morphology, Fe and Sm oxidation states, the oxidation resistance and magnetic properties of pure and Sm doped Fe_3O_4 nanoparticles were studied. TEM and XRD results show that Sm doped Fe_3O_4 nanoparticles have a good dispersion and are smaller than pure Fe_3O_4 nanoparticles. The Fe and Sm oxidation states of pure and Sm doped Fe_3O_4 nanoparticles were studied by means of XANES analysis. The magnetic properties of Sm doped Fe_3O_4 nanoparticles determined by VSM exhibit superparamagnetic behavior with high saturation magnetization. It was found that Sm doping in a small amount makes it possible not only to reduce the sizes of magnetite nanoparticles but also to improve their oxidation resistance and increase their saturation magnetization value. These pure and Sm doped Fe_3O_4 magnetic nanoparticles are expected to be used in a number of biomedical applications.

DOI: 10.1134/S1995078018020088

INTRODUCTION

Nanotechnology is showing a big potential for biomedical and pharmacological applications [1–5]. Magnetic nanoparticles (NPs) are believed to be one of the most important classes of nanomaterials. The magnetic properties of these NPs based on their inducible magnetization and superparamagnetic behavior allow researchers to deliver them to a defined location and to manipulate them in the presence of an external magnetic field. Magnetic Fe_3O_4 NPs have been of great interests because of their biocompatibility and low toxicity, which makes them highly attractive in many aspects of oncology. Moreover, being small in size and having large surface area-to-volume ratio allows them to absorb compounds such as small molecules, drugs, DNA, RNA, and proteins [6–9]. These magnetic NPs can find a number of applications for targeted drug delivery of biological molecules and drugs [10], magnetic hyperthermia [11] as well as in magnetic resonance imaging (MRI) [12] as contrast agents to visualize tumors [13, 14]. To date, self-antitumor activity of magnetic NPs and magnetic fluids as well as how to achieve the antitumor effect and complete regression of malignant tumors has not been clearly understood [2]. One of the major drawbacks of magnetite NPs is their instability to oxidation as they are easily oxidized in the air even at room temperature, which results in significant loss of their magnetic properties [3]. The substitution of the Fe ions with doping rare earth atoms in Fe_3O_4 NPs may improve their magnetic properties and enhance their resistance to oxidation [15, 16]. Doping may also reduce the size and change the shape and surface morphology of these NPs [15]. The surface coating of NPs with a coating agent reduces the tendency of NPs to agglomerate, and gives a possibility to functionalize them [17]. Sodium dodecylbenzenesulfonate can be used as a biocompatible capping agent to control the size distribution and prevent the agglomeration of magnetic NPs, and help to obtain magnetic NPs with the improved superparamagnetic properties [15].

Numerous chemical methods have been developed for the synthesis of magnetite NPs, such as solvothermal, hydrothermal, mechanochemical and electrochemical as well as microemulsions, sol-gel techniques, the thermal decomposition of the salts, co-precipitation of a mixture of ferrous and ferric iron compounds [18–24]. The most common method is the co-precipitation from an aqueous medium. This technique usually results in the formation of particles smaller than 20 nm having superparamagnetic properties [18]. However, this kind of synthesis limits a precise control over their size and morphology [24]. The synthesis of magnetite nanoparticles with well controlled morphology and particle size distribution is usually carried out using the high-temperature solvothermal method [19]. However, it should be noted, that solvothermal synthesis takes a long period of time

[1]The article is published in the original.

to be carried out in a closed reactor, which hampers the adjustment of the synthesis. In comparison with the conventional synthesis, the microwave assisted synthesis relies on the efficient energy transformation and uniform heat distribution in the reaction system, which results in obtaining higher reaction rates, chemical yields, good reliability and reproducibility [24].

This paper focuses on the synthesis of pure and Sm doped Fe_3O_4 NPs using the microwave assisted synthesis technique in the presence of non-toxic and biocompatible sodium dodecylbenzenesulfonate as a coating agent in an aqueous solution. The synthesized MNPs were characterized employing several experimental methods. The structure and morphology, Fe and Sm oxidation states, oxidation resistance and magnetic properties of pure and Sm doped Fe_3O_4 NPs were studied.

EXPERIMENTAL DETAILS

Reagents

In our experiments, all the reagents were analytically graded and used without any further purification. The chemicals iron(III) chloride hexahydrate ($FeCl_3 \cdot 6H_2O$), sodium acetate trihydrate ($CH_3COONa \cdot 3H_2O$) ethylene glycol (EG), and polyethyleneglycol (PEG), sodium dodecylbenzenesulfonate (SDBS), samarium oxide, (Sm_2O_3) were purchased from Sigma-Aldrich and used as received.

The Synthesis of Pure and Sm Doped Fe_3O_4 Nanoparticles

The preliminary synthesis of samarium chloride was synthesized from samarium oxide. A certain amount of Sm_2O_3 was mixed with the concentrated hydrochloric acid solution, then the mixture was heated at 80–90°C till the reaction solution changed from turbid to clear. After that, the excess hydrochloric acid was evaporated and dried in exposure beaker, the obtained $SmCl_3$ was dissolved in ethanol, and then recrystallized.

The synthesis of pure Fe_3O_4 NPs was performed with the use of microwave irradiation. The synthesis procedure was as follows: the compounds $FeCl_3 \cdot 6H_2O$ (0.7661 g), $NaAc \cdot 3H_2O$ (2.0400 g), SDBS (1.3939 g) and PEG (0.42 mL) were added in ethylene glycol (25.0 mL) to form homogeneous mixture under stirring at room temperature. Then, the mixture was sealed with a silicone stopper in a glass vial and was placed in the microwave oven (CEM Discover SP, USA). After that, the mixture was heated and maintained at fixed 200°C for 1 h with continuous stirring, then cooled down to room temperature. The black particles were separated from the solution by magnetic separation, washed three times with absolute ethanol and dried in a vacuum oven at 60°C for several hours. In comparison with the conventional solvothermal or hydrothermal synthesis of magnetite NPs, the reactions using the microwave irradiation technique have higher reaction rates, which allow reducing the synthesis time from 6 up to 1 h.

For the synthesis of Sm doped Fe_3O_4 NPs, the total amount of doping Sm^{3+} was 11.25 wt %. The total amount of doping element was chosen from the assumption that samarium did not form secondary phases in the magnetite structure, and to estimate the maximum effect of doping. The compounds $FeCl_3 \cdot 6H_2O$ (0.3830 g), $SmCl_3 \cdot 6H_2O$ (0.0216 g) $NaAc \cdot 3H_2O$ (2.0400 g), SDBS (1.3939 g) and PEG (0.42 mL) were used with the same temperature and time of synthesis as in the described above procedure. The amount of sodium acetate trihydrate, SDBS and PEG remained unchanged as in the synthesis of pure Fe_3O_4 nanoparticles. The microwave oven used for the synthesis of pure and Sm doped Fe_3O_4 NPs operated with microwave power at 200 W and at a frequency of 2450 MHz.

Characterization Techniques

Transmission electron microscopy. Transmission electron microscopy (TEM) images were obtained using the FEI Tecnai G2 Spirit Bio TWIN microscope operating at accelerating voltage of 120 kV.

X-ray diffraction. Pure and Sm doped Fe_3O_4 NPs were characterized by XRD to determine their structure and estimate the average size of nanoparticles. The X-ray diffraction patterns of the samples were recorded on the ARL X'TRA diffractometer (Thermo Fisher Scientific) using Cu$K\alpha$ (1.5406 Å) radiation at room temperature in the range of 15° to 80° in the 2θ scale, with a scanning rate of 6 deg/min and a step size 0.02°.

X-ray absorption near edge structure. The oxidation state and oxidation resistance of pure and Sm doped Fe_3O_4 NPs were studied by means of X-ray absorption near edge spectra (XANES). The Fe K-edge XANES spectra of the reference samples of iron oxides and the obtained nanoparticles were measured using the laboratory Rigaku R-XAS Looper X-ray spectrometer operating in transmission mode. A Ge(311) Johansson-type bent single crystal was used as a monochromator. The samples were measured as prepared and a month later, in order to study their oxidation resistance. About 8 mg of powder samples were mixed uniformly in a boron nitride matrix and pressed into pellets ~13 mm in diameter and 2 mm thick, for obtaining a unit step jump at the Fe K-edge edge. The XAS data were processed by standard procedures using the Iffefit software package [25] to obtain the normalized X-ray absorption near edge structure (XANES) spectra.

Magnetization measurements. Magnetic curves M (H) were measured using a vibrating sample magnetometer LakeShore VSM 7400. Experiments were car-

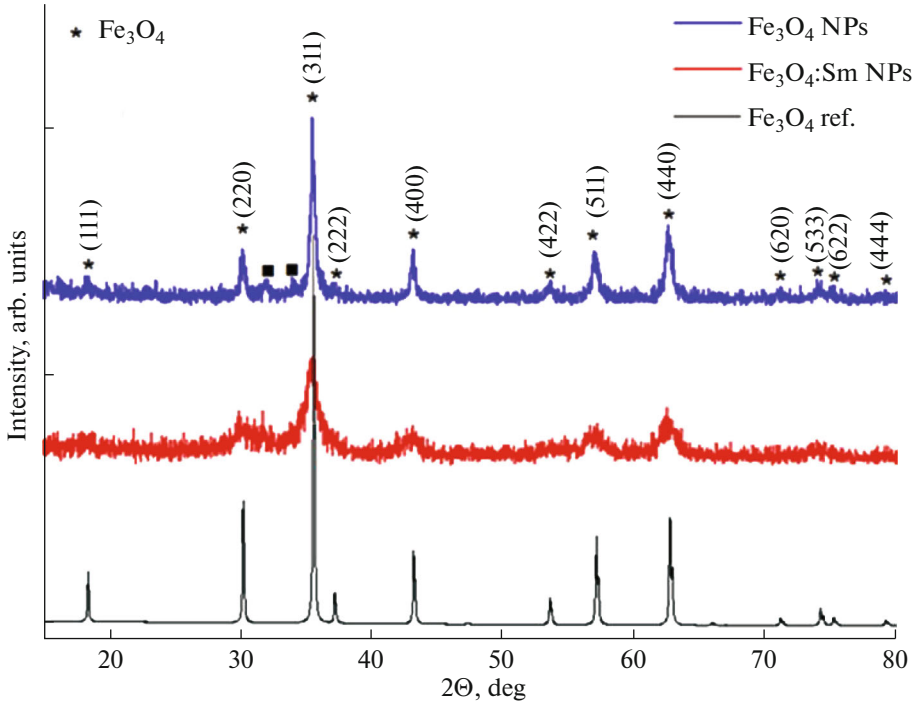

Fig. 1. (Color online) XRD patterns of pure and Sm doped Fe_3O_4 NPs synthesized by microwave synthesis with the reference Fe_3O_4 pattern (Pdf-2 card no. 880315).

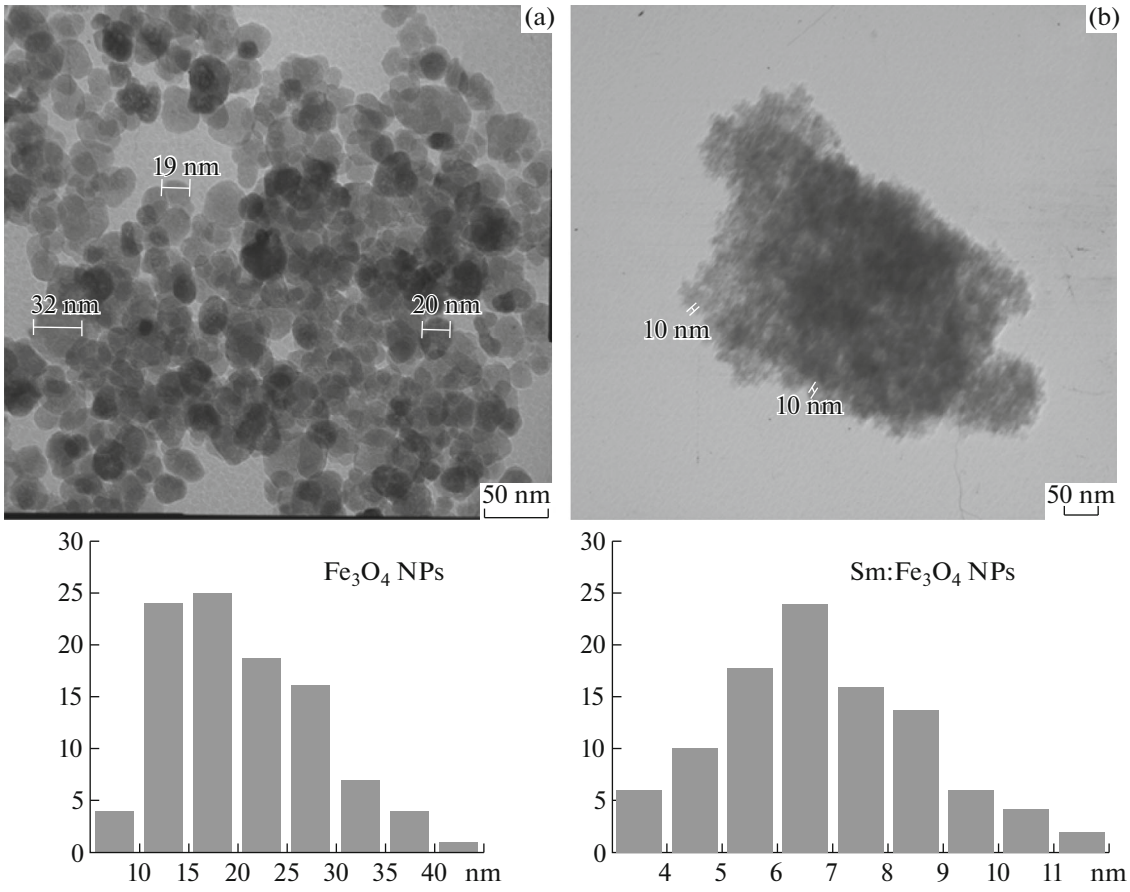

Fig. 2. TEM images of (a) pure and (b) Sm doped Fe_3O_4 NPs.

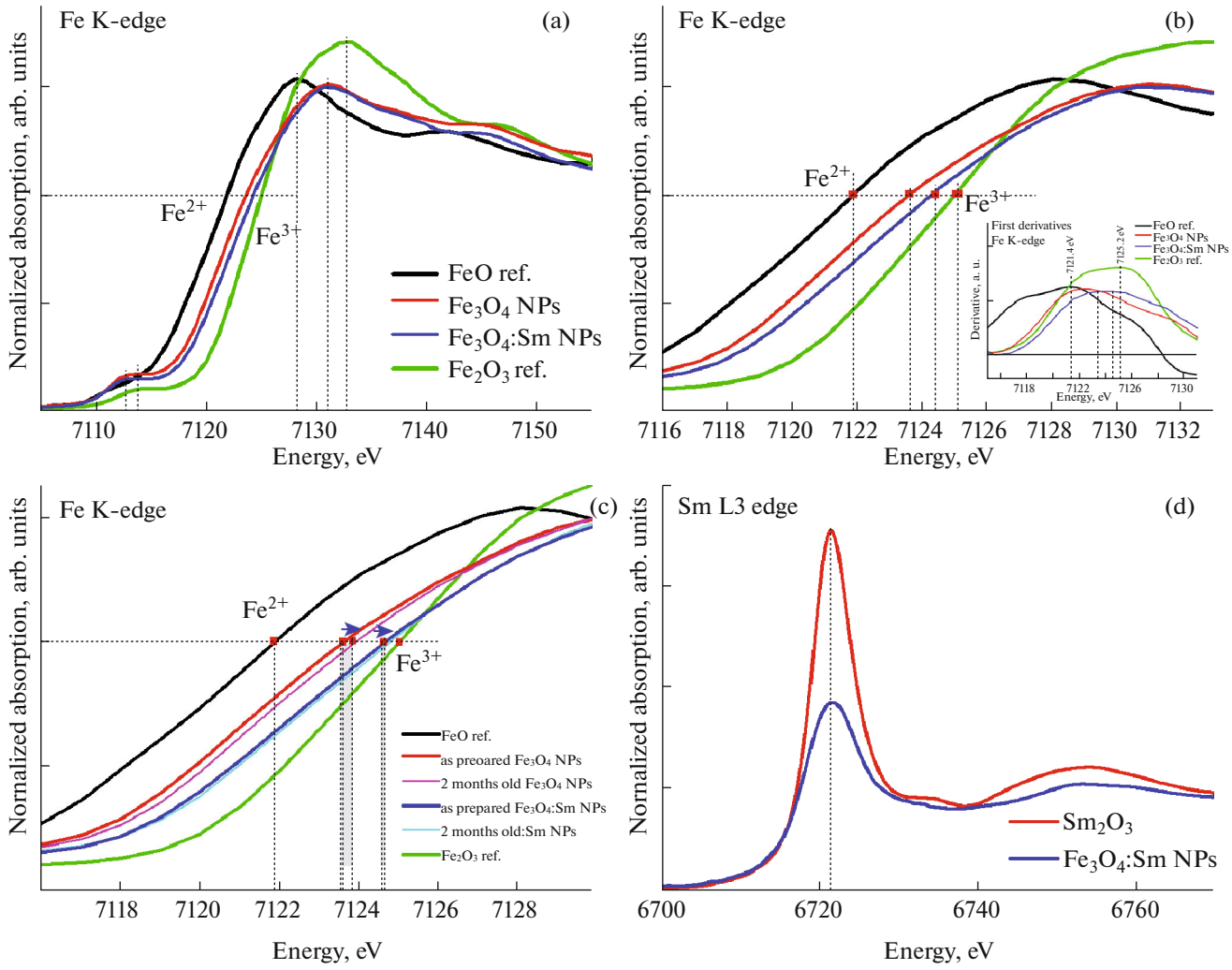

Fig. 3. (Color online) (a) Fe K-XANES spectra of pure and Sm doped Fe_3O_4 NPs in comparison with Fe oxides references; (b) Fe K-edge region and the positions of the absorption edges; the inset with the spectra of first derivatives of the XANES spectra in the Fe K-edge region; (c) oxidation of pure and Sm doped Fe_3O_4 NPs; (d) Sm L_3-XANES spectra of Sm doped Fe_3O_4 NPs in comparison with Sm_2O_3 reference compound.

ried out in magnetic field up to 10 kOe at room temperature (295 K). The samples in a form of powder were placed and tightly pressed in between two parts of polymer capsules with spherical bottom size about ∅ 4.5 mm. The samples masses were 5–17 mg. The polymer capsule contribution to magnetic signal was negligible. The magnetization error due to the sample shape was below 5%, which was controlled by rotation of the sample. The mass measurement error was less than 1%.

RESULTS AND DISCUSSION

The XRD patterns of pure and Sm doped Fe_3O_4 NPs obtained by microwave assisted synthesis are shown in Fig. 1. All peaks are consistent with the reference Fe_3O_4 pattern (Pdf-2 card no. 880315). However, Fe_3O_4 and Fe_2O_3 have the same spinel structure and their XRD peak positions are quite close to each other. The presence of a particular phase cannot be ruled out on the basis of XRD pattern only. Hence, the XANES analysis was used to determine the formal structure and oxidation state of iron and samarium in the synthesized nanoparticles. The XRD pattern can be used to estimate an average particle size. It is clearly seen that the full width at half maximum (FWHM) of all reflection peaks increased and the intensity of the peaks decreased after adding the dopant Sm cations, which indicates the decrease in their average particle size. The average size of the pure Fe_3O_4 NPs estimated from the Debye–Scherrer formula was 29 nm and for the Sm doped Fe_3O_4 NPs it was 8.6 nm, i.e., approximately three times smaller than that of pure Fe_3O_4 NPs.

Table 1. Magnetic parameters of pure and Sm doped Fe_3O_4 NPs

Nanoparticles	M_s (emu/g)	H_c (T)	M_r (emu/g)
Pure Fe_3O_4 NPs	74.9	0.0075	14.96
Sm doped Fe_3O_4 NPs	122.1	0.0001	0.30

The Transmission Electron Microscopy images of the pure and Sm doped Fe_3O_4 NPs are shown in Figs. 2a, 2b, respectively. It was observed that the particle size of pure magnetite nanoparticles does not exceed 40 nm, and when doping MNPs, the particle size decreases. These data indicate that samarium is embedded in or deposited on the surface of the iron oxide particles and impedes their growth. The particle size distribution appears to be quite narrow and the particle shape is reasonably spherical. The Fig. 2a indicates that pure Fe_3O_4 NPs have a diameter of approximately 30 nm and the Fig. 2b shows that Sm doped Fe_3O_4 NPs have a diameter of approximately 10 nm, which almost agrees with the average crystallite size obtained from XRD data analysis.

XANES characterization was carried out to probe the oxidation states of iron and samarium and oxidation resistance of the pure and Sm doped Fe_3O_4 NPs. The energy position of the XANES spectra depends on the binding energy of the absorbing atom, and hence, on the oxidation state of the absorbing atom. The absorption edges of iron oxides shift to higher energy positions with the increment of iron oxidation state. Figure 3a shows the normalized Fe K-edge XANES spectra of pure and Sm doped Fe_3O_4 NPs in comparison with the iron reference compounds (FeO and α-Fe_2O_3). Figure 3b shows the position of the Fe absorption edges of freshly prepared pure and Sm doped Fe_3O_4 NPs and the reference compounds. The absorption edge energy position was defined as the position of the maximum of the first derivative in the absorption edge region. The inset of the Fig. 3b indicates the position of the maximum of the first derivatives of the XANES spectra in the Fe K-edge region.

For FeO, the absorption edge of iron atoms is located at 7121.6 eV, with a quite weak pre-edge peak observed at 7112 eV. For Fe_2O_3, the absorption edge is located at 7125.0 eV, with a broad pre-edge peak at 7114 eV. For spinel Fe_3O_4, iron ions have a mixed valence of +2 and +3, with Fe^{2+} ions at the tetrahedral sites and Fe^{3+} ions at the octahedral sites, therefore the iron ions have a mean oxidation state of +2.67. For the synthesized pure and Sm doped Fe_3O_4 NPs, the absorption edges are located at 7123.8 and 7124.6 eV, illustrating that the iron ions in pure and Sm doped Fe_3O_4 NPs have the oxidation states of $+2.65 \pm 0.1$ and $+2.88 \pm 0.1$, respectively. Different values of the mean oxidation state of pure and Sm doped NPs are attributed to different particle sizes, because nanoparticles of smaller size contain more Fe^{3+} ions. In Fig. 3c, the shift of the absorption edge of pure and Sm doped Fe_3O_4 NPs after the synthesis and a month later reveals the oxidation of the nanoparticles. The width of that shift indicates the velocity of the oxidation. The arrows in Fig. 3c illustrate the shift of the absorption edge by 0.3 and 0.1 eV and the change of oxidation state from +2.65 to +2.74 and from +2.88 to +2.91, respectively. Pure Fe_3O_4 NPs were oxidized faster than Sm doped Fe_3O_4 NPs, and hence, the samarium doping enhances their resistance to oxidation. Figure 3d shows the normalized Sm L_3-edge XANES spectra of Sm doped Fe_3O_4 NPs and Sm_2O_3 reference sample. In the case of Sm L_3-edge XANES spectra, the absorption edge position is equal to that of Sm^{3+} in Sm_2O_3, but the peak profiles of Sm doped Fe_3O_4 NPs are somewhat not fully identical to that of Sm_2O_3 in the

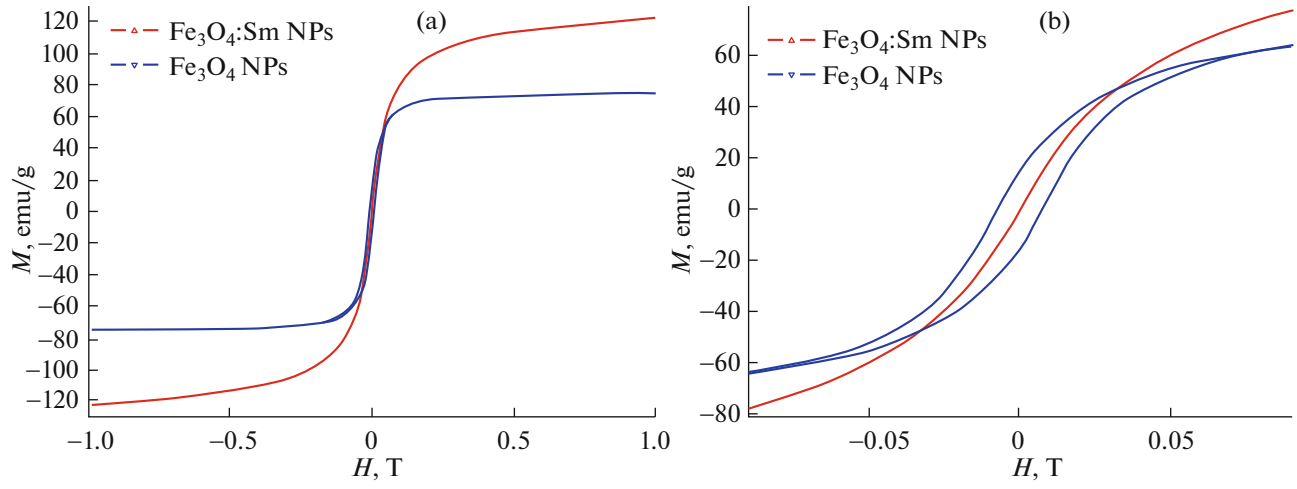

Fig. 4. (Color online) Magnetization curves $M(H)$ of pure and Sm doped Fe_3O_4 NPs at room temperature.

intensity of the white line, the shape of the features and their positions. This indicates that Sm ions in magnetite NPs are mainly Sm^{3+}.

The magnetic behavior of the pure and Sm doped Fe_3O_4 NPs was investigated with a vibrating sample magnetometer (VSM). As shown in Fig. 4a the saturation magnetization value (M_s) of the pure Fe_3O_4 NPs (~75 emu/g) are lower than that of Sm doped Fe_3O_4 NPs (~122 emu/g). As can be seen from Fig. 4b, the magnetic coercivity (H_c) and remanence (M_r) are relatively zero, which indicates a superparamagnetic behavior of the Sm doped Fe_3O_4 NPs. The magnetic parameters of pure and Sm doped Fe_3O_4 NPs are presented in Table 1.

CONCLUSIONS

In summary, sodium dodecylbenzenesulfonate coated pure and Sm^{3+} doped Fe_3O_4 NPs with relatively uniform size distribution were successfully prepared via microwave assisted synthesis. Their structure, Fe and Sm ion oxidation states, oxidation resistance and magnetic properties were evaluated using TEM, XRD, XANES, and VSM techniques. It was found that Sm doped Fe_3O_4 nanoparticles were smaller than pure Fe_3O_4 NPs. Doping nanoparticles with samarium leads to the decrease in their sizes. The average size of pure Fe_3O_4 NPs was about 29 nm and Sm doped Fe_3O_4 NPs was about 8 nm, so the size of Sm doped Fe_3O_4 NPs was approximately three times smaller than that of pure Fe_3O_4 NPs. The average oxidation states of iron and samarium were determined. The small amount of Sm^{3+} ions enhanced the oxidation resistance of magnetite nanoparticles. In addition, such a substitution significantly enhances magnetic properties of Sm doped Fe_3O_4 nanoparticles via magnetoelectric interaction, and the augmented magnetization value. The prepared Sm doped Fe_3O_4 nanoparticles were found to have a superparamagnetic behavior with saturation magnetization value of 122 emu/g which allows their manipulation with an external magnetic field for desired biomedical applications.

ACKNOWLEDGMENTS

This work was supported by Ministry of Education and Science of the Russian Federation (agreement no. 14.587.21.0027, unique identifier RFMEFI58716X0027).

REFERENCES

1. L.H. Reddy, J.L. Arias, J. Nicolas, and P. Couvreur, "Magnetic nanoparticles: design and characterization, toxicity and biocompatibility, pharmaceutical and biomedical applications," Chem. Rev. **112**, 5818–5878 (2012).
2. A. K. Gupta and M. Gupta, "Synthesis and surface engineering of iron oxide nanoparticles for biomedical applications," Biomaterials **26**, 3995–4021 (2005).
3. S. Laurent, D. Forge, M. Port, A. Roch, C. Robic, L. Elst, and R. Muller, "Magnetic iron oxide nanoparticles: synthesis, stabilization, vectorization, physicochemical characterizations, and biological applications," Chem. Rev. **108**, 2064–2110 (2008).
4. D. Ling, N. Lee, and T. Hyeon, "Chemical synthesis and assembly of uniformly sized iron oxide nanoparticles for medical applications," Acc. Chem. Res. **48**, 1276–1285 (2015).
5. C. Xu and S. Sun, "New forms of superparamagnetic nanoparticles for biomedical applications," Adv. Drug Deliv. Rev. **65**, 732–743 (2013).
6. G. Liu, J. Gao, H. Ai, and X. Chen, "Applications and potential toxicity of magnetic iron oxide nanoparticles," Small **9**, 1533–1545 (2013).
7. H. Markides, M. Rotherham, and A. J. El Haj, "Biocompatibility and toxicity of magnetic nanoparticles in regenerative medicine," J. Nanomater. **2012**, 614094 (2012).
8. F. Alexis, E. M. Pridgen, R. Langer, and O. C. Farokhzad, Nanoparticle technologies for cancer therapy, in *Handbook of Experimental Pharmacology* (Springer, Berlin, Heidelberg, 2010).
9. S. Nie, Y. Xing, G. J. Kim, and J. W. Simons, "Nanotechnology applications in cancer," Ann. Rev. Biomed. Eng. **9**, 257–288 (2007).
10. J. Klostergaard and C. E. Seeney, "Magnetic nanovectors for drug delivery," Nanomed.: Nanotechnol., Biol., Med. **8**, S37–S50 (2012).
11. D. Yoo, J.H. Lee, T. H. Shin, and J. Cheon, "Theranostic magnetic nanoparticles," Acc. Chem. Res. **44**, 863–874 (2011).
12. C. Chouly, D. Pouliquen, I. Lucet, J. J. Jeune, and P. Jallet, "Development of superparamagnetic nanoparticles for MRI: effect of particle size, charge, and surface nature on biodistribution," J. Microencapsulat. **13**, 245–255 (1996).
13. C. Li, "A targeted approach to cancer imaging and therapy," Nat. Mater. **13**, 110–115 (2014).
14. J. Xie, G. Liu, H. S. Eden, H. Ai, and X. Chen, "Surface-engineered magnetic nanoparticle platforms for cancer imaging and therapy," Acc. Chem. Res **44**, 883–892 (2011).
15. W. Huan, C. Cheng, Y. Yang, H. Yuan, and Y. Li, "A study on the magnetic and photoluminescence properties of $Eu(n^+)$ and Sm^{3+} doped Fe_3O_4 nanoparticles," J. Nanosci. Nanotechnol. **12**, 4621–4634 (2012).
16. Y. Liu and N. Zhang, "Gadolinium loaded nanoparticles in theranostic magnetic resonance imaging," Biomaterials **33**, 5363–5375 (2012).
17. W. Wu, Q. He, and C. Jiang, "Magnetic iron oxide nanoparticles: synthesis and surface functionalization strategies," Nanoscale Res. Lett. **3**, 397–415 (2008).

18. X. Wang, J. Zhuang, Q. Peng, and Y. Li, "A general strategy for nanocrystal synthesis," Nature (London, U.K.) **437**, 121–124 (2005).

19. W. Zhang, F. Shen, and R. Hong, "Solvothermal synthesis of magnetic Fe_3O_4 microparticles via self-assembly of Fe_3O_4 nanoparticles," Particuology **9**, 179–186 (2011).

20. T. Iwasaki, R. Nakatsuka, K. Murase, H. Takata, H. Nakamura, and S. Watano, "Simple and rapid synthesis of magnetite/hydroxyapatite composites for hyperthermia treatments via a mechanochemical route," Int. J. Mol. Sci. **14**, 9365–9378 (2013).

21. A. B. Chin and I. I. Yaacob, "Synthesis and characterization of magnetic iron oxide nanoparticles via w/o microemulsion and Massart's procedure," J. Mater. Process. Technol. **191**, 235–237 (2007).

22. S. Sun and H. Zeng, "Size-controlled synthesis of magnetite nanoparticles," J. Am. Chem. Soc. **124**, 8204-5 (2002).

23. D. Ramimoghadam, S. Bagheri, and S. B. A. Hamid, "Progress in electrochemical synthesis of magnetic iron oxide nanoparticles," J. Magn. Magn. Mater. **368**, 207–229 (2014).

24. C. Li, Y. Wei, A. Liivat, Y. Zhu, and J. Zhu, "Microwave-solvothermal synthesis of Fe_3O_4 magnetic nanoparticles," Mater. Lett. **107** 23–26 (2013).

25. B. Ravel and M. Newville, "ATHENA, ARTEMIS, HEPHAESTUS: data analysis for X-ray absorption spectroscopy using IFEFFIT," J. Synchrotr. Rad. **12**, 537–541 (2005).